J Sol-Gel Sci Technol (2011) 59:145–152
DOI 10.1007/s10971-011-2472-1

ORIGINAL PAPER

Influence of PEG additive and annealing temperature on structural and electrochromic properties of sol–gel derived WO_3 films

Yanqun Fang · Xilian Sun · Hongtao Cao

Received: 19 October 2010 / Accepted: 22 April 2011 / Published online: 5 May 2011

Abstract Sol–gel derived tungsten oxide (WO_3) films have been deposited by spin coating route using acetylated peroxotungstic acid (APTA) or a mixture of APTA and polyethylene glycol (PEG) dissolved in ethanol as the precursor solution, followed by thermal treatment in air. The influence of PEG additive and annealing temperature on the structural and electrochromic (EC) behavior of the films have been investigated. For films annealed at 300 °C, a porous nanocrystalline/amorphous microstructure was obtained in the WO_3-PEG film, while monoclinic microstructure was formed in the pure WO_3 film. Moreover, for the WO_3-PEG films, the film microstructure was found to depend on the annealing temperature. Electrochemical studies indicate that the WO_3-PEG film annealed at 300 °C (WP-300) exhibits superior EC properties, which produces faster switching speed ($t_c = 19$ s, $t_b = 3$ s),better reversibility ($K = 0.97$) as well as higher optical modulation ($\Delta T = 32\%$ at 550 nm) and coloration efficiency ($\eta = 22$ cm^2/C at 550 nm). Our results suggest that PEG addition in combination with an appropriate annealing treatment can benefit the EC properties, arising from the ease of ion diffusion within the EC material, as evident from the nanocrystallines embedded into the amorphous matrix with a porous character.

Keywords Tungsten oxide · Electrochromic · Acetylated peroxotungstic acid · Polyethylene glycol · Sol–gel · Annealing temperature

Y. Fang · X. Sun · H. Cao (✉)
Ningbo Institute of Materials Technology and Engineering (NIMTE), Chinese Academy of Sciences (CAS), 315201 Ningbo, People's Republic of China
e-mail: h_cao@nimte.ac.cn

1 Introduction

Electrochromic (EC) materials have attracted considerable attention due to their various applications, for example, in smart windows, antiglare mirrors, and high contrast displays [1]. It is intriguing that they can be reversibly switched between two different optical states by alternately applying positive and negative electrical voltages. As one of cathodic inorganic EC materials, tungsten oxide (WO_3) is the most intensively investigated EC material [2, 3]. Up to now, many techniques, such as sol–gel method [4, 5], solvothermal method [6, 7], sputtering [8, 9], electrodepostion [10, 11], etc., have been successfully used to prepare tungsten oxides. The sol–gel route has been widely adopted owing to its low cost and better reproducibility in terms of stoichiometry, crystallinity, porosity, thickness, etc [12]. Among various sol–gel routes for making WO_3 based precursor material, peroxo-route (wherein tungsten metal is dissolved in hydrogen peroxide to form peroxotungstic acid, which is called PTA product) is superior because it can avoid the incorporation of the unwanted impurity such as Na^+ and the preparation is easy to operate [13]. The films stemming from PTA-based precursor solution are easily dehydrated, deoxidized and polymerized by thermal treatment [12]. During its synthesis, PTA can be further modified by the addition of an organic acid to the reaction mixture to yield its acid derivative called acetylated peroxotungstic acid (APTA), which possesses excellent solubility in polar solvents so as to stabilize the solution and to facilitate the formation of WO_3 films [14, 15].

To color a tungsten oxide film, dual injection of electrons from the back contact and small positive charge ions (H^+, Li^+, Na^+ and K^+) from an electrolyte is necessary. Take Li^+ as an example, the reaction resulting in the reversible coloration of the WO_3 film is

$$WO_3(\text{transparent}) + xLi^+ + xe^- \leftrightarrow Li_xWO_3(\text{blue}), \quad (1)$$

while electrons injection into the WO_3 film is very rapid, diffusion of Li^+ ions within the WO_3 film is so kinetically slow that it becomes the limiting factor of the above reaction (1). By this token, electrochromic properties are tightly associated with the grain size and the fraction of void space (film porosity characteristic) in WO_3 film that affect the ion diffusion rate severely. Compared to crystalline WO_3 films, non-crystalline (amorphous) films have been found to exhibit excellent EC properties arising from its large specific surface area [16–18]. However, amorphous films suffer from irreversible performance degradation due to structural modifications, while crystalline WO_3 is much more stable due to denser structure and slower dissolution rate in electrolytes. To overcome this drawback, nano-structured WO_3 with large specific surface area is expected to improve EC performance of crystalline counterpart, which is named nanocrystalline WO_3. It is reported that the nano-scale particles are able to expand much more easily and have better accommodation of the structural strain caused by the electrochemical reaction of lithium. Previous studies have described the electrochromic behavior of nanocrystalline WO_3 films which show comparable EC properties and higher stability compared to the conventional amorphous counterpart [19, 20].

There are distinct variations in the microstructural and electrochromic properties of the films upon varying the composition of the sol–gel precursor or/and post-deposition annealing conditions [16]. Moreover, appropriate post-deposition annealing could enhance the adhesive force between the film and the substrate. Sun et al. [21] had investigated the properties of nanocrystalline WO_3 films obtained from colloidal sols containing diverse amounts of oxalic acid dehydrate (OAD). The evolution of the microstructure and electrochromic properties of the sol–gel derived nanostructured tungsten oxide films upon varying polyethylene glycol (PEG) content in the precursor solutions was also studied [22]. However, the investigations concerning the structural and electrochromic properties of sol–gel derived WO_3 films as a function of annealing temperature were seldom reported.

In the present work, sol–gel derived tungsten oxide films were deposited by spin coating using APTA or a mixture of APTA and PEG dissolved in ethanol as the precursor solution, followed by thermal treatment in air. The role of PEG additive in controlling crystal growth and film porosity and its resultant effect on EC properties have been discussed. Besides, the influence of annealing temperature on structural and EC behavior of the WO_3 films with PEG addition (the WO_3-PEG films) has also been investigated.

2 Experimental

2.1 Preparation of precursor solutions and tungsten oxide films

13 g of tungsten metal powder was slowly added to 80 ml of 30% hydrogen peroxide solution placed in a 5 °C water bath. The clear solution obtained upon filtration was further refluxed at 55 °C for 12 h after addition of 80 ml of acetic anhydride, in order to acetylate the peroxotungstic acid and remove the excess hydrogen peroxide completely. The resulting milk white solution was centrifuged at 8,000 rpm for 15 min and the precipitate was then vacuum-dried at 60 °C to obtain a pale yellow solid of acetylated peroxotungstic acid (APTA). 1 g of APTA was dissolved in 10 ml of ethanol by magnetic stirring to yield the precursor solution. Then 0.3 g of polyethylene glycol (PEG, with molecular weights of 2,000) was added to form the APTA-PEG precursor solution.

These solutions were then spin coated onto fluorine doped tin oxide (FTO) glasses at 2,000 rpm for 30 s. The film formed by the APTA precursor solution was dried at 100 °C and then annealed in air at 300 °C for 3 h to obtain the pure WO_3 film (named W-300 hereafter). In order to study the temperature effect, the WO_3-PEG films prepared from the APTA-PEG precursor solution were thermally treated at 100 °C and then subjected to a heat treatment at 250 °C, 300 °C and 350 °C for 3 h, respectively. For convenience, we shall refer to these films as WP-250, WP-300, and WP-350, respectively.

2.2 Characterization techniques

Thermogravimetric/differemtial thermal analysis was carried out in air at a heating rate of 10 °C/min between 20–500 °C (Pyris Dimond TG-DTA, Perkin-Elmer Company). Fourier transform infrared (FT-IR) spectra were recorded as KBr pellets on a Thermo Nicolet 6700 Explorer. The thin film structure were determined by X-ray diffraction (XRD) with a Bruker D8 Advance diffractometer using Cu Ka ($\lambda = 1.5406$ Å) radiation and transmission electron microscopy (TEM, Tecnai G2 F20, FEI company). The film thickness and refractive index measurements were obtained via a variable angle spectroscopic ellipsometer (J.A.Woollam Co., Inc). Transmittance spectra of the colored and bleached films were recorded in the 300–2,000 nm wavelength range in a Lambda 950 spectrophotometer. Electrochemical characteristics were measured in a three-electrode electrochemical cell (AUTOLAB PGSTAT302) with platinum sheet as the counter electrode, WO_3 film deposited on a FTO coated glass substrate as the working electrode, Ag/AgCl/KCl as the reference electrode, and 1 M $LiClO_4$ in propylene carbonate as the electrolyte, respectively.

3 Results and discussion

3.1 Structure analysis

To clearly describe the structural evolution of the PEG-containing WO_3 gel with heating, the TG-DTA results of the PEG-containing WO_3 gel and the changes of the IR spectra with heating are exhibited in Figs. 1 and 2, respectively. The TG curve in Fig. 1 shows weight changes mainly in two steps at 20–150 °C (~25%) and 150–300 °C (~20%), respectively. The weight decrease in the first step is mainly attributed to the desorption of the surface water and ethanol, which is consistent with the endothermic peak below 100 °C in the DTA curve [23]. Meanwhile the decomposition of peroxo species, corresponding to the first exothermic peak at ~105 °C, also results in the decrease. Furthermore, the weight decrease in the second step is caused by the decomposition of PEG-2000, corresponding to the exothermic peak at ~255 °C, which reveals that organic matter is burning at this temperature and WO_3 phase starts to change from amorphous to crystalline. Another exothermic peak at ~435 °C in the DTA curve indicates the crystallization to monoclinic WO_3. The FT-IR spectra of the various temperature treated PEG-containing WO_3 gel also demonstrate the structural changes along with the TG-DTA results. As displayed in Fig. 2, the PEG-containing WO_3 gel heated at 250 °C presents characteristic absorption bands corresponding to W–O stretch (~660 cm^{-1}), bridging peroxide (~880 cm^{-1}), W=O terminal stretch (~980 cm^{-1}), bending vibration of C–H (1,500 ~ 1,300 cm^{-1}), and hydroxyl group (~1,610 cm^{-1}), which suggests that it is composed of various structural units of W–O–W, W–O–O–W, W=O, C–H, W–OH, etc. [24]. The C–H groups, as one of the signals coming from PEG, disappear when the annealing temperature goes to 300 °C and 350 °C. The intensity of the W–O–O–W and W–OH absorption bands decreases with the increasing heating temperature, while the W–O–W and W=O bands are always present and can be detected at 300 °C and above.

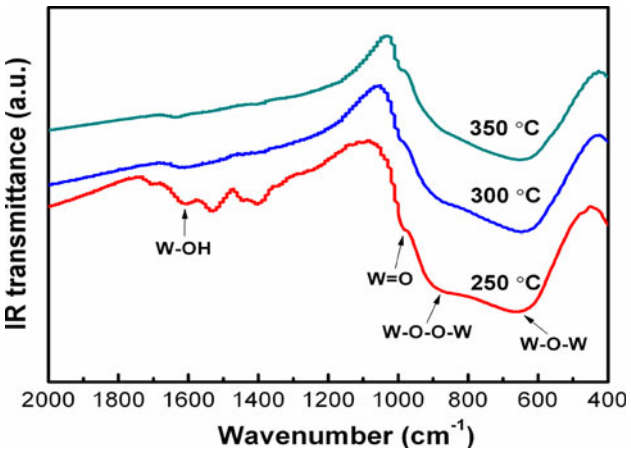

Fig. 2 FT-IR spectra of the PEG-containing WO_3 gel, depending on the heat treatment conditions

All the tungsten oxide films after the final thermal treatment are transparent, and the film thicknesses are found to be around 130 ± 15 nm. Figure 3 exhibits the structural evolution of the WO_3-PEG films as a function of temperature in the range of 250–350 °C along with the crystal structure of W-300. No other discernible peaks but only diffraction peaks assigned to FTO are observed, revealing the amorphous nature of the WP-250 film (Fig. 3b). For the films annealed at 300 °C, the WP-300 film (Fig. 3c) features nanocrystalline, supported by the presence of two very weak diffraction peaks at $2\theta = 23.6°$ and 24.4° that are corresponding to (020) and (200) plane, respectively. In this case, one can assume that the WO_3 nanocrystals were embedded in the amorphous WO_3 matrix, as illustrated in Fig. 4 [25]. However, relative to

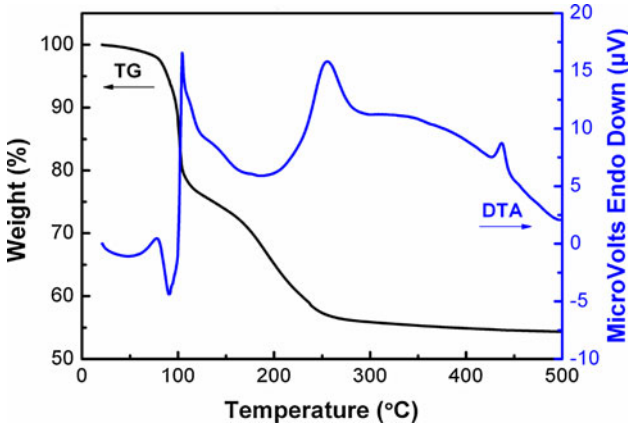

Fig. 1 Thermal analysis profiles of the PEG-containing WO_3 gel

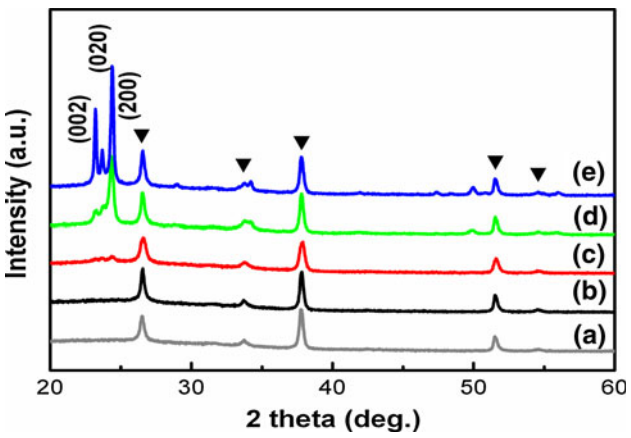

Fig. 3 XRD patterns of the FTO-glass **a** and WO_3 films of WP-250 **b**, WP-300 **c**, WP-350 **d** and W-300 **e**; (*black filled Triangle*) peaks arise from the underlying substrate

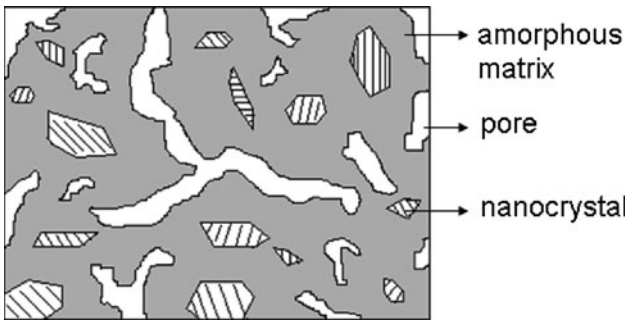

Fig. 4 Schematic of the WP-300 film with a porous nanocrystalline/amorphous structure

the WP-300 film, the crystallization of the W-300 film (Fig. 3e) is more complete because three extra peaks around $2\theta = 23.7°$ are sketched out. With the annealing temperature increasing to 350 °C, the WP-350 film (Fig. 3d) is well-crystallized, as indicated by the three characteristic reflections of monoclinic WO_3. PEG is thus presumed to act as a drying control chemical additive as it regulates the rate of solvent removal from the film and could delay the crystallization temperature of tungsten oxide film [26]. Moreover, the WP-350 film exhibits a preferred (200) orientation, so the addition of PEG can also modulate the growth direction of WO_3 grains.

Further structural characterizations of the WO_3 samples were performed by TEM and the selected area electron diffraction (SAED). As shown in Fig. 5a, b, there are only diffuse rings in the SAED patterns, which indicate the absence of well-ordered crystalline structure in WP-250 and WP-300. Comparatively, the clear SAED patterns from Fig. 5c, d reveal that WP-350 and W-300 are crystalline. So it is inferred from these results that the WO_3-PEG films and the pure WO_3 films get crystallized at 350 °C and 300 °C, respectively, in good agreement with the XRD results shown in Fig. 3.

Not only controlling the crystal growth, PEG additive also promotes to form the pore structure of WO_3 film. Porosity is reflected by the relative density P which is estimated as the ratio of the density of the film and the bulk ($P = \rho_f/\rho_b$). The Lorentz-Lorentz relationship for the relative density P is given by the following relation [27]:

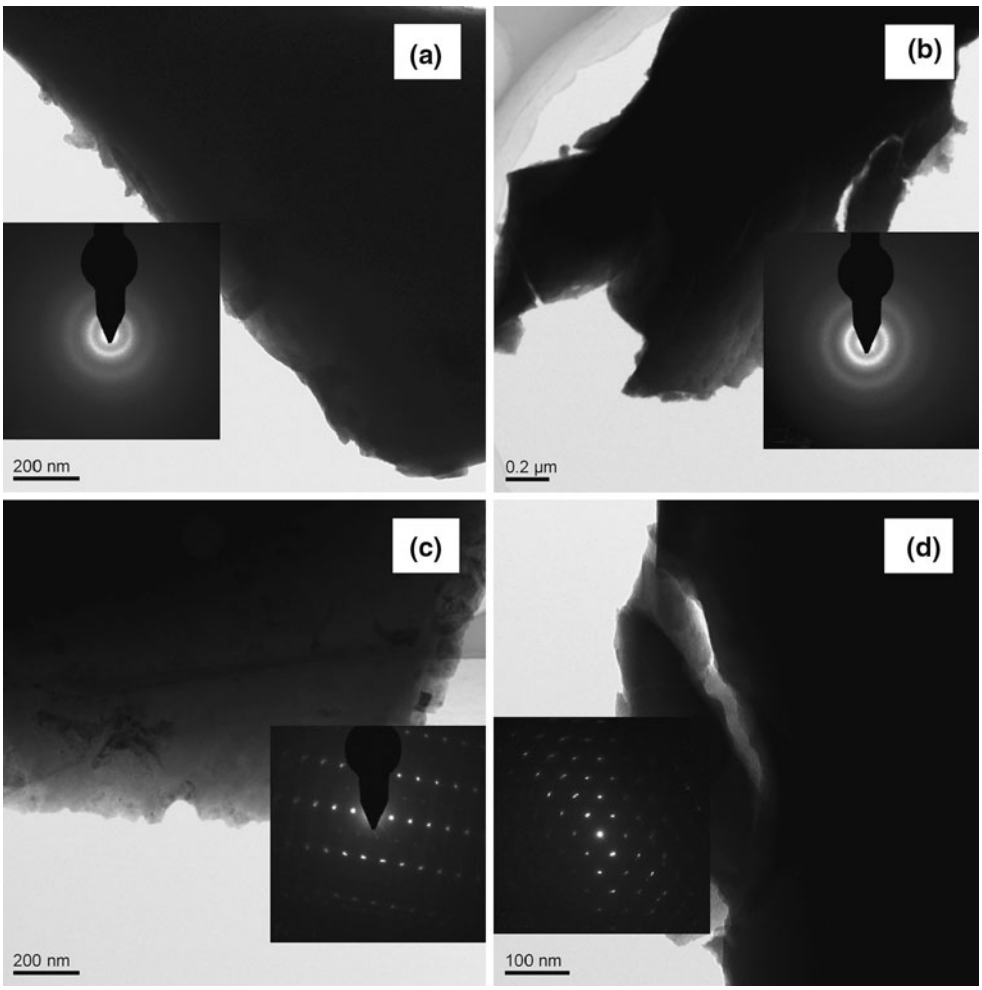

Fig. 5 TEM images of the WO_3 samples of WP-250 **a**, WP-300 **b**, WP-350 **c** and W-300 **d** and their corresponding SAED patterns (*the inset*)

$$P = \left(\frac{n_f^2 - 1}{n_f^2 + 1}\right)\left(\frac{n_b^2 + 1}{n_b^2 - 1}\right), \quad (2)$$

where n is the refractive index at 550 nm, and the subscripts f and b refer to the film and the bulk (the refractive index of bulk WO_3 at 550 nm is 2.5 [28]), respectively. As shown in Fig. 6, on one hand, the refractive index of W-300 (blue line) is greater than that of WP-300 (red line) in the wavelength ranging from 500 to 950 nm. Hence the relative density of W-300 is greater than that of WP-300 according to Eq. 2. This result confirms the effect of PEG on increasing the porosity of the film. On the other hand, Fig. 6 also displays a decreasing n for the WO_3-PEG films with increasing annealing temperature, in coordination with a decrease of relative density P as the annealing temperature rises. In particular, the relative density at 550 nm calculated from Eq. 2 are 0.838, 0.831, 0.751 and 0.904, corresponding to WP-250, WP-300, WP-350 and W-300, respectively.

3.2 Electrochromic properties

Cyclic voltammograms of the WO_3 samples recorded in the range of ±1.0 V at a scan speed of 20 mV/s are shown in Fig. 7, and the inserted histogram that demonstrates the integral areas under the curve of these tungsten oxide films is also displayed. It is well known that the voltammogram area is directly related to the ion storage capacity of the film, which could be expressed as:

$$Q = S/v, \quad (3)$$

where Q is the charge density (C/cm^2), S is the area, and v is the sweep rate (V/s). It is clearly seen that the area of the WP-300 film (red block) is larger than that of the W-300 film (blue block), and their ion storage capacities (Q) derived from Eq. 3 are found to be 22 and 9 mC/cm^2, respectively. This can be attributed to the more porosity

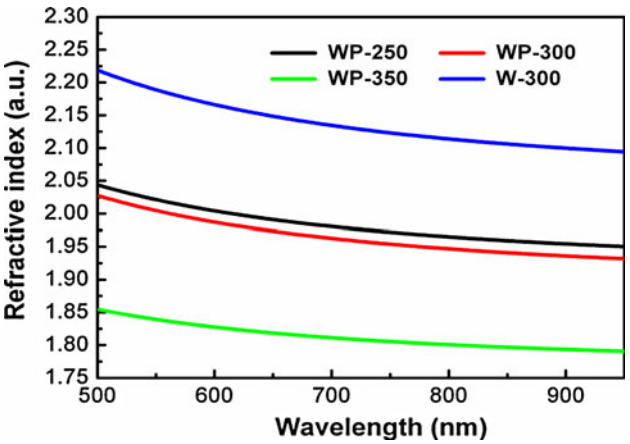

Fig. 6 The comparison of refractive index for the WO_3 films

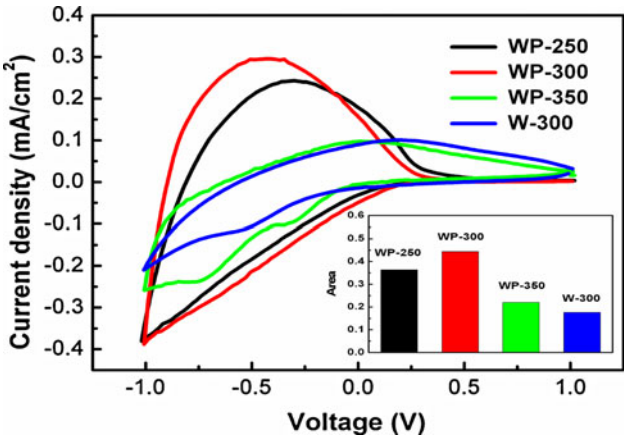

Fig. 7 Cyclic voltammograms of the WO_3 films recorded in the range of ±1.0 V at a scan speed of 20 mV/s in a 1 M $LiClO_4$-PC electrolyte

and nanocrystalline feature of the WP-300 film. Besides, the influence of annealing temperature on the voltammograms of the WO_3-PEG films is also compared (Fig. 7). It is noted that the voltammogram area of WP-300 (red block) is bigger than that of WP-250 (black block), indicating that the ion storage capacity enhances by the elevation of temperature from 250 °C to 300 °C, in line with the more porous structure of WP-300. As the temperature continuously increasing to 350 °C, however, the area (green block) decreases and the calculated ion storage capacity is 11 mC/cm^2. It is attributed to the higher annealing temperature-reinforced crystallization of the host film which provides higher activation energy barrier for Li^+ ion to intercalate into the film. Further studies on probing the Li^+ ions transporting behavior are undergoing (e.g., in situ temperature-dependent ion diffusion), in order to approach the fundamental aspects of the diffusion kinetics.

The diffusion coefficient for Li^+ ions can be calculated from the peak anodic current using Randles-Servicik equation [29]:

$$i_p = 2.72 \times 10^5 \times n^{3/2} \times D^{1/2} \times C_0 \times v^{1/2}, \quad (4)$$

where i_p is the peak anodic current density (A/cm^2), $n = 1$ is the number of electrons, D the diffusion coefficient (cm^2/s), C_0 the concentration of the active ion in solution (mole/cm^3), and v the sweep rate (V/s). The diffusion coefficient D is calculated according to Eq. 4 and summarized in Table 1. It is noted that the Li^+ ion diffusion coefficients of the W-300 and WP-300 films are 6.8×10^{-12} and 5.9×10^{-11} cm^2/s, respectively. One order of magnitude higher diffusion coefficient of WP-300 manifests its improved response time. The large surface area and short Li^+ diffusion path of nanocrystallites, along with its porous structure of the 300 °C annealed WO_3-PEG film can account for its superior

Table 1 Electrochromic properties of the sol–gel derived WO_3 film samples

Samples	D (cm^2/s)	t_c (s)	t_b (s)	Q (mC/cm^2)	K	ΔT (%, @550 nm)	η (cm^2/C, @550 nm)
WP-250	4.0×10^{-11}	20	3	18	0.93	31	20
WP-300	5.9×10^{-11}	19	3	22	0.97	32	22
WP-350	6.5×10^{-12}	22	17	11	0.63	9	5
W-300	6.8×10^{-12}	22	16	9	0.79	8	5

electrochemical kinetics. In addition, Li^+ ion diffusion coefficients of the WO_3-PEG films annealed at different temperature are compared in Table 1, from which the WP-300 film shows a little higher diffusion coefficient than that of the WP-250 film, but the Li^+ diffusion coefficient of WP-350 is one order of magnitude smaller relative to the above two samples. The optimal annealing temperature to obtain the best Li^+ ion diffusion coefficient for the WO_3-PEG films is 300 °C in our study, which is closely related to the complicated microstructural evolution, in particular, local structure information.

The reversibility of the WO_3 film during the electrochemical reactions, which is closely related to electrochemical stability of the WO_3 film, is defined by the ratio between extracted/inserted charge ($K = Q_{ex}/Q_{in}$) in the cyclic voltammogram, as listed in Table 1. Compared to the W-300 film, the WP-300 film exhibits higher reversibility. For the WO_3-PEG films, it is observed that the electrochemical reversibility approaches 97% @300 °C, and whether increasing or decreasing the temperature would deteriorate the reversibility. The lower value of the insertion reversibility indicates that more Li^+ ions are getting trapped in the framework [30].

Switching time characteristics between the colored and bleached states for the WO_3 samples are calculated from chronocoulometry data with a square potential of ±1.0 V. The response time of coloration (t_c) and bleaching (t_b) is defined as the time required for 90% of the full optical change during coloration and bleaching processes, respectively. As seen in Table 1, the WP-300 film shows faster coloration and bleaching kinetics than those of the W-300 film. In respect to the WO_3-PEG films, the effect of annealing temperature on the response time is also investigated. It is found that the WP-250 and WP-300 films show comparable coloration/bleaching time, while further increasing the temperature to 350 °C slows down the response time. This can be explained by the small diffusion coefficient of Li^+ ions in the well-crystallized films which severely slows down the kinetics of the electrochemical process [31].

The transmittances ranging from 300 nm to 2,000 nm of the WO_3 films in the colored and bleached states are illustrated in Fig. 8a. After applying a constant current density of 0.33 mA/cm^2 of Li^+ ions for 30 s (i.e., ~ 10 mC/cm^2), the maximum transmittance of the colored W-300 film is 73% at 494 nm. Besides, the maximum transmittance observed for the bleached W-300 film is 78% at 517 nm after extracting the same amount of Li^+ ions. For the colored state of WO_3-PEG films, WP-250, WP-300 and WP-350 each has a maximum value of 60, 62 and 77% at 422, 421 and 473 nm, respectively. Correspondingly, the observed maximum transmittances for the bleached WP-250, WP-300 and WP-350 are 84, 80 and 82% at 609, 592 and 528 nm, respectively. Then the transmittance modulations calculated from the transmittance differences between the colored and bleached states ($\Delta T = T_b - T_c$) are illustrated in Fig. 8b, as the transmittance modulation (ΔT) has been recognized as

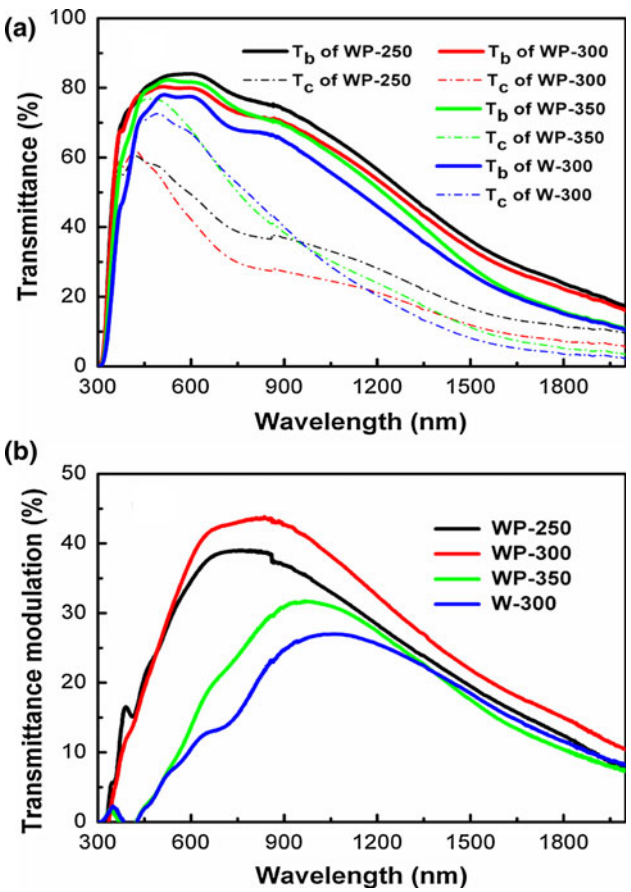

Fig. 8 Transmittances of the colored and bleached states **a** and transmittance modulations **b** of the WO_3 films

one of the most important criterions for the EC materials. ΔT of the WP-300 film varies between 19 and 43% in the 450–800 nm range, while ΔT of the W-300 film has a variation of 2–19%, which reveals that the former exhibits superior optical characteristics. In addition, WP-250 and WP-350 each has a transmittance modulation variation of 21–39% and 2–27%, respectively. WP-250 shows a transmittance modulation comparable to WP-300, but in the case of the WP-350 film, the value of ΔT decreases. These observations are in concordance with the above-mentioned EC data which are all significantly related to the microstructure of these WO_3 films. For clarity, ΔT values at 550 nm of these samples are displayed in Table 1.

Coloration efficiency (CE) is defined as the change in the optical density with charges intercalated per unit electrode area, which has been recognized as another important criterion for the electrochromic materials. It can be calculated according to the formula [32]:

$$\mathrm{CE}(\eta) = \log(T_b/T_c)/q, \quad (5)$$

where T_b and T_c are the transmittance of the film in the bleached and colored states, and q is the charge density (C/cm^2). According to Fig. 9, CEs of all the films increase with the wavelength in the visible range. For the WP-300 film, the coloration efficiency increases from 12 to 40 cm^2/C, corresponding to the wavelength from 450 to 800 nm, while the coloration efficiency of W-300 is within the range from 1 to 14 cm^2/C. The addition of PEG enables the 300 °C annealed WO_3 film to form nanocrystalline grains in the amorphous tungsten oxide matrix, thus improves the coloration efficiency of this film. Furthermore, coloration efficiencies of the WO_3-PEG samples annealed at 250 °C and 350 °C are calculated to be in the range of 13–31 cm^2/C and 1–19 cm^2/C, respectively. The CE values of the WO_3-PEG films are found to follow the trend: CE (WP-300) > CE (WP-250) > CE (WP-350), from which one can be reminiscent of aforementioned sorting: ΔT (WP-300) > ΔT (WP-250) > ΔT (WP-350), and K (WP-300) > K (WP-250) > K (WP-350). It is believed that the porous nanocrystalline/amorphous structure, like the case of the WP-300 sample, provides easier access of a large amount of Li^+ into the film which ensures an amplification of the optical response as well as the coloration efficiency. The improved electrochromic performance of WP-300, such as coloration efficiency and optical response time, is considerably better than those of vacuum sputtered WO_3 films [3, 33], and also comparable to other reported sol–gel prepared WO_3 films [25, 34].

Apart from CE and response time, the practical reproducibility of repeated coloring and bleaching is another important criterion for evaluating the EC materials, which is especially essential for the practical application. Figure 10 exhibits the reliability of WP-300 by cyclic voltammogram with 500 cycles of back and forth switching between the colored and bleached states. At the beginning of the whole cycles, the charge density drops a little to some extent with the intercalation and extraction of Li^+ ions. However, the CV curves of WP-300 after 100 cycles maintain the similar shape with a slight increment of the charge density as the cycle number increasing, indicating the film possesses a good practical reproducibility.

4 Conclusions

Using APTA or a mixture of APTA and PEG dissolved in ethanol as the precursor solution, pure WO_3 (W-300) or WO_3-PEG (WP-250, WP-300 and WP-350) films were processed by spin coating and thermal treatment in air. The role of PEG in the acetylated peroxotungstic acid precursor solution is critical as it modulates the structure of the WO_3 films and consequently their EC properties effectively. The presence of PEG facilitates the formation of

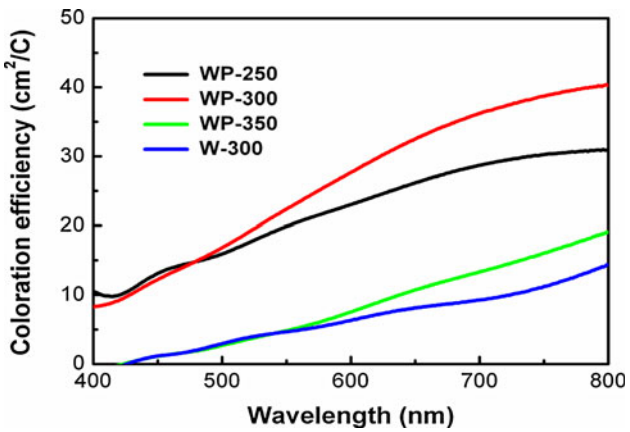

Fig. 9 The comparison of coloration efficiency for the WO_3 films in the visible range

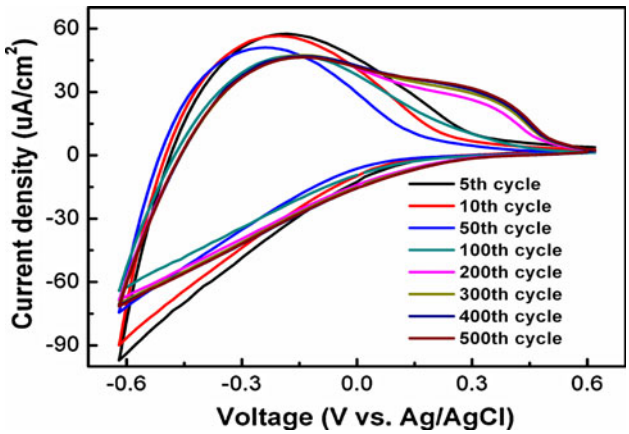

Fig. 10 Cyclic voltammograms of WP-300 recorded in the range of ±0.6 V at a scan speed of 20 mV/s in a 1 M $LiClO_4$-PC electrolyte

nanocrystalline phase in the WO_3-PEG film when annealed at 300 °C. Owing to the large surface area, short Li^+ diffusion path of nanocrystallites, and the porosity character, WP-300 exhibits better EC performance such as faster response time, larger ion storage capacity, better reversibility, as well as higher transmittance modulation and coloration efficiency in the visible range relative to W-300 prepared from the APTA precursor solution. Further, considerable attention has been paid to the influence of annealing temperature on the structural and EC behavior of the WO_3-PEG films. X-ray diffraction analysis clearly reveals that the WP-250, WP-300 and WP-350 films have amorphous, combined nanocrystalline/amorphous and crystalline structure, respectively, which is further supported by the TEM and SAED characterizations. As a result, EC properties are somewhat improved by the elevation of temperature from 250 °C to 300 °C, nevertheless the WP-350 film exhibits fairly poorer EC properties than those of the WP-250 and WP-300 films, which is due to its well-crystallized structure. The above work suggests that PEG addition together with an appropriate annealing temperature promote the WO_3 film to form a porous nanocrystalline/amorphous mosaic structure, which can basically account for the improved electrochromic properties.

Acknowledgments The authors are grateful for the financial support of the CAS/SAFEA International Partnership Program for Creative Research Teams, and the aided program for Science and Technology Innovative Research Team of Ningbo Municipality (2009B21005).

References

1. Lampert CM (2003) Sol Energy Mater Sol Cells 76:489
2. Deb SK (2008) Sol Energy Mater Sol Cells 92:245
3. Granqvist CG (1995) Handbook of inorganic electrochromic materials. Elsevier, Amsterdam
4. Deepa M, Joshi AG, Srivastava AK, Shivaprasad SM, Agnihotry SA (2006) J Electrochem Soc 153:C365
5. Yang B, Barnes PRF, Bertram W, Luca V (2007) J Mater Chem 17:2722
6. Yoo SJ, Lim JW, Sung YE, Jung YH, Choi HG, Kim DK (2007) Appl Phys Lett 90:173126
7. Houx NL, Pourroy G, Camerel F, Comet M, Spitzer D (2010) J Phys Chem C 114:155
8. Karuppasamy A, Subrahmanyam A (2007) J Appl Phys 101:113522
9. Wang SJ, Chen CH, Ko RM, Kuo YC, Wong CH, Wu CH, Uang KM, Chen TM, Liou BW (2005) Appl Phys Lett 86:263103
10. Deepa M, Srivastava SA, Singh S, Agnihotry SA (2004) J Mater Res 19:2576
11. Srivastava AK, Deepa M, Singh S, Kishore R, Agnihotry SA (2005) Solid State Ion 176:1161
12. Sharma N, Deepa M, Varshney P, Agnihotry SA (2000) J Sol–Gel Sci Tech 18:167
13. Kudo T, Okamoto H, Matsumoto K, Sasaki Y (1986) Inorg Chim Acta 111:L27
14. Cronin JP, Agrawal A, Tarico DJ, Tonazi JCL (1996) US patent #5,525,264
15. Munro B, Kramer S, Zapp P, Krug H (1998) J Sol–Gel Sci Tech 13:673
16. Taylor DJ, Cronin JP, Allard LF, Birnie DP (1996) Chem Mater 8:1396
17. Deepa M, Saxena TK, Singh DP, Sood KN, Agnihotry SA (2006) Electrochim Acta 51:1974
18. Subrahmanyam A, Karuppasamy A (2007) Sol Energy Mater Sol Cells 91:266
19. Wang JM, Khoo E, Lee PS, Ma J (2008) J Phys Chem C 112:14306
20. Djaoued Y, Priya S, Balaji S (2008) J Non-Cryst Solids 354:673
21. Sun M, Xu N, Cao YW, Yao JN, Wang EG (2000) J Mater Res 15:927
22. Deepa M, Kar M, Singh DP, Srivastava AK, Ahmad S (2008) Sol Energy Mater Sol Cells 92:170
23. Choy JH, Kim YI, Yoon JB, Choy SH (2001) J Mater chem 11:1506
24. Orel B, Groselj N, Krasovec UO, Jese R (2002) J Sol–Gel Sci Tech 24:5
25. Wu WT, Liao WP, Chen LY, Chen JS, Wu JJ (2009) Phys Chem Chem Phys 11:9751
26. Cremonesi A, Djaoued Y, Bersani D, Lottici PP (2008) Thin Solid Films 516:4128
27. Hitchman ML (1979) Thin Solid Films 61:341
28. Karuppasamy KM, Subrahmanyam A (2009) J Phys D Appl Phys 42:095301
29. Deepa M, Srivastava AK, Kar M, Agnihotry SA (2006) J Phys D Appl Phys 39:1885
30. Sun XL, Cao HT, Liu ZM, Li JZ (2009) Appl Surf Sci 255:8629
31. Agrawal A, Cronin JP, Zhang R (1993) Sol Energy Mater Sol Cells 31:9
32. Granqvist CG (1991) Materials science for solar energy conversion systems. Pergamon, Oxford
33. Washiizu E, Yamamoto A, Abe Y, Kawamura M, Sasaki K (2003) Solid State Ion 165:175
34. Wu WT, Liao WP, Chen JS, Wu JJ (2010) Chem Phys Chem 11:3306